

Morphology and Properties of Microcapsules with Different Core Releases

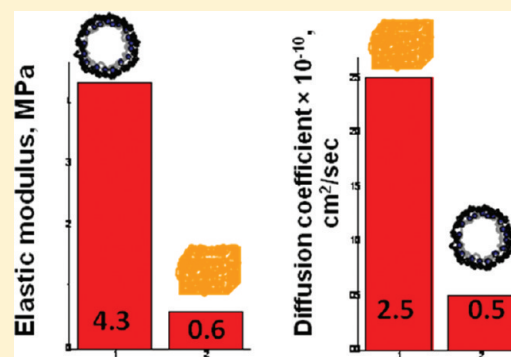
Olga Shchepelina,[†] Milana O. Lisunova,[†] Irina Drachuk, and Vladimir V. Tsukruk*

School of Materials Science and Engineering, Georgia Institute of Technology, Atlanta, Georgia 30332, United States

Supporting Information

ABSTRACT: The morphology, mechanical properties, and permeability of hydrogen-bonded layer-by-layer (LbL) microcapsule shells assembled on cubic CdCO₃ cores have been studied in comparison with traditional shells assembled on spherical SiO₂ cores. We observed that the morphology of LbL shells is dramatically affected by the different release processes with highly porous and softened LbL shells as a result of the intense CO₂ gas formation and ion release during the removal of cubic CdCO₃ cores. A substantial increase in porosity is reflected in a dramatic change in the mesh size of LbL shells, from 2 nm for spherical capsules to above 35 nm for cubic capsules. Shells also possess enhanced permeability with a many fold increase in diffusion coefficient for dextran molecules and enhanced softening with the elastic modulus dropping by almost an order of magnitude for cubic capsules. These dramatic changes in shell morphology, porosity, permeability, and stiffness, observed in this study for the first time, are all important for the intelligent projection of controlled loading and unloading behavior of microcontainers with different shapes and composition, a component usually overlooked in current studies.

KEYWORDS: layer-by-layer microcapsules, shell morphology, porosity, permeability, elastic modulus



INTRODUCTION

Thin shell LbL microcapsules are one class of micro- and nanocarriers, which is of great interest for current research because of their ability for controlled storage and release of different compounds, as well as the potential to act as synthetic cell-like structures.^{1–4} These capsules may be incorporated in drug delivery systems,^{5,6} microreactors,^{7,8} and catalytic systems.⁷ Polymer microcapsules, which can be formed by the coating of selected cores followed by core dissolution, are proposed for prospective applications in enzymatic catalysis and as a platform for the construction of artificial cells and organelles, among many other applications.^{9,10} Their unique characteristics such as low specific density, high specific surface area, potential for high loading capacity, controlled permeability, stiffness, and enhanced catalytic and binding activities are extremely intriguing for further studies.^{11–15}

The advantage of these synthetic structures is that their properties can be tailored and designed to respond to specific stimuli, which trigger the release of their content at a desired site and time. Also complex multicompartamental microcapsules can be created and used as building blocks in the fabrication of complex capsules for multifunctional delivery.¹⁶ To date, it has been demonstrated that such polymer microcapsules can be loaded with a variety of molecules of interest: macromolecular drugs, lipids,¹⁷ dendrimers,¹⁸ enzymes,¹⁹ DNA,²⁰ and viruses.²¹

LbL assembly is a well-established method used to build such polymer micro- and nanoshells around different organic, inorganic, and biological cores with fine control over

composition, thickness, mechanical properties, and functionality.^{3,4,22–32} In this method, multilayered coatings are formed on various cores through a sequential adsorption of properly matched species—biological molecules, polymers, organic molecules, and nanoparticles—able to interact via electrostatic interactions, hydrogen-bonding, covalent bonding, and bio-specific interactions.³³ The organic and inorganic core material can be removed afterward by dissolution³⁴ or calcination¹ to leave a hollow capsule. To fabricate intact capsules consisting only of the shell material used during the coating, core dissolution should result in complete elimination of the core without affecting the LbL shells, although the task of complete core removal seems to be complicated from chemical point of view. Capsule properties depend strongly on the choice of polyelectrolytes employed and adsorption conditions, such as ionic strength, temperature, solvent composition, and number of layers; however, it is important to note that these properties are also considerably affected by the selection of core material.

At present, a variety of cores have been exploited to template hollow capsules. One class includes organic cores made of water-insoluble materials, such as melamine formaldehyde (MF)-cores dissolvable at low pH and in some organic solvents, polystyrene (PS) cores soluble in tetrahydrofuran, and biofriendly polylactic acid/polylactic-co-glycolic acid

Received: September 19, 2011

Revised: March 5, 2012

Published: March 5, 2012

(PLA/PLGA) cores soluble in an acetone/*N*-methyl-2-pyrrolidinone mixture.³⁵ In spite of the technologically well-established process of synthesis, their drawbacks include sticking of the core material to the capsule wall. Naturally, the oligomers formed upon dissolution can easily entangle with polyelectrolyte (PE) multilayer, making their removal difficult even after several washing cycles. As shown by Gao et al.,³⁶ the residues of MF in hollow polyelectrolyte capsules was shown to reach 30% of the capsule weight. The osmotic stress occurring upon dissolution of MF-cores may rupture the PE multilayer shell. In some cases, the capsule stays intact during the dissolution process only if it is assembled with no more than 8–10 PE layers.^{36,37} The mentioned processes bring uncertainty in further study of permeability properties of the capsules fabricated on the polymeric templates.

Another class of cores employed for microcapsule fabrication combines both ionic and molecular crystals soluble in acidic, basic, or organic solvent. At present, different carbonate particles (e.g., CaCO_3 , CdCO_3 , and MnCO_3)^{38,39} and SiO_2 particles⁴⁰ have been used for polyelectrolyte multilayer templating. A number of inorganic cores such as CaCO_3 ,^{41,42} MnCO_3 , CdCO_3 ,⁴³ or SnS ⁴⁴ have also been employed as nonspherical templates for preparation of anisotropic hollow capsules. The advantage of inorganic cores is the low molecular weight of the ions diffusing out during the dissolution of the core, which minimizes osmotic stress and LbL shell disruption. The inorganic core is assumed to be completely eliminated during dissolution steps and does not affect morphology of LbL shells during release. These capsules can be comprised of a high number of layers and have permeability lower than that of the latex-templated capsules, which supports the formation of an intact capsule wall.

It is generally suggested but rarely confirmed that the employment of different core materials results in different morphologies and physical properties such as permeability, which is crucial for loading and unloading behavior. However, there are no direct comprehensive studies on how core type and the dissolution process affect the morphology, porosity, permeability, and stiffness of the resultant LbL capsules.

Hence, in this study, we focus on properties of LbL shells of hollow microcapsules such as porosity, permeability, and stiffness and how these properties are affected by core chemistry and release process. Specifically, we employed three types of cores: regular spherical silica particles, cubic CdCO_3 particles, and mixed MnCO_3 cores. We focused on the spherical silica and cubic CdCO_3 particles due to the significant difference in chemical properties and shape. Shape and chemical composition were considered as factors determining the properties of the final capsules. We demonstrated that these two types of cores with different release methods produce very different shell morphologies and physical properties despite the fact that both spherical and cubic LbL shells possess the same chemical composition and assembly processes (Figure 1). We suggest that the core dissolution regarding CdCO_3 , which involves CO_2 gas formation and intense ion release, dramatically affects shell morphology by increasing shell mesh size from 2 to 35 nm, thereby increasing permeability/diffusion coefficient by 5-fold, and decreasing the stiffness by about an order of magnitude. Such dramatic differences in LbL properties observed here draw attention to the critical importance of the nature of cores and release procedure on final morphology and properties of LbL shells after core removal in contrast to general expectations and suggestions on

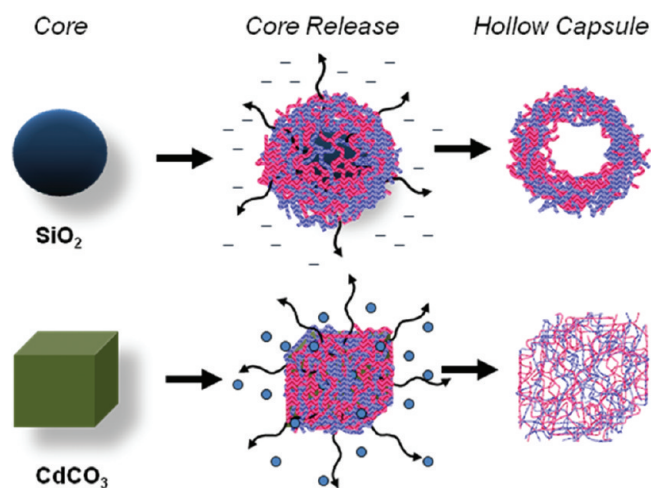


Figure 1. Schematic illustration of microcapsule preparation.

similar properties of polymeric LbL shells with identical chemical composition and assembly process unrelated to the nature of core and core release.

EXPERIMENTAL SECTION

Materials. Tannic acid (1700 Da), PVPON (1 300 000 Da), branched polyethyleneimine (PEI) (25 000 Da), and mono- and dibasic sodium phosphate were purchased from Sigma-Aldrich. Cadmium nitrate tetrahydrate (Alfa Aesar) and urea (Alfa Aesar) were used as received. Silica particles with diameter $4.0 \pm 0.2 \mu\text{m}$ as 10% dispersions in water were obtained from Polysciences, Inc. Fluorescein isothiocyanate (FITC) labeled dextrans (4, 70, 250, 500 kDa) and unlabeled dextran-70 kDa were purchased from Sigma-Aldrich. Hydrofluoric acid (HF 48–51%) was purchased from Aristar. Ultrapure water (Nanopure system) with a resistivity of $18.2 \text{ M}\Omega \text{ cm}$ was used in all experiments. Single-side polished silicon wafers of the {100} orientation (University Wafer) were cut with a standard of $10 \text{ mm} \times 20 \text{ mm}$ and cleaned in a piranha solution, as described elsewhere.⁴⁵

Preparation of Cadmium Carbonate Particles. Cadmium carbonate crystals were synthesized by addition of one part of 2 M cadmium nitrate to one part of 4 M urea solution in a Pyrex round-bottom flask with a Teflon-lined screw cap.⁴⁶ The urea and cadmium nitrate solutions were purged with nitrogen before mixing. The mixture was aged at $80 \text{ }^\circ\text{C}$ for 16 h using a constant-temperature oil bath. The precipitate was isolated from the supernatant solution by filtration through Nuclepore track-etch membranes ($0.4 \mu\text{m}$ pore size, Whatman) and washed twice with Nanopure water.

Preparation of Manganese Carbonate Particles. Manganese carbonate crystals were prepared by mixing MnSO_4 and NH_4HCO_3 solutions.⁴⁷ First, a nanoseed solution was prepared by mixing 20 mg of NH_4HCO_3 with 1 mg of MnSO_4 in 100 mL of DI water under rapid stirring. Then, 250 mL of 6 mM MnSO_4 (with 0.5% 2-propanol) was mixed with 250 mL of 0.06 M NH_4HCO_3 (with 0.5% 2-propanol) and stirred at $80 \text{ }^\circ\text{C}$. Prior to mixing, 37.5 mL of nanoseed solution was added to MnSO_4 solution. The precipitate was extensively washed with Nanopure water and dried in air. Scanning electron microscopy (SEM) analysis revealed formation of cubic and spherical particles.

Preparation of LbL Capsules. PEI (TA/PVPON) microcapsules with varied number of layers have been fabricated according to the established procedure described elsewhere.⁴⁸ First, a precursor, PEI, was allowed to adsorb onto silica, cadmium carbonate, or manganese carbonate particles in a 0.5 mg/mL aqueous solution (0.1 M NaCl, pH = 7) for 15 min followed by the deposition of hydrogen-bonded TA/PVPON layers in a 1 mg/mL 0.01 M phosphate buffer solution (pH = 5). During LbL deposition, particles were redispersed in the appropriate solution by gentle shaking for 15 min. After deposition of each layer, particles were collected by centrifugation and washed

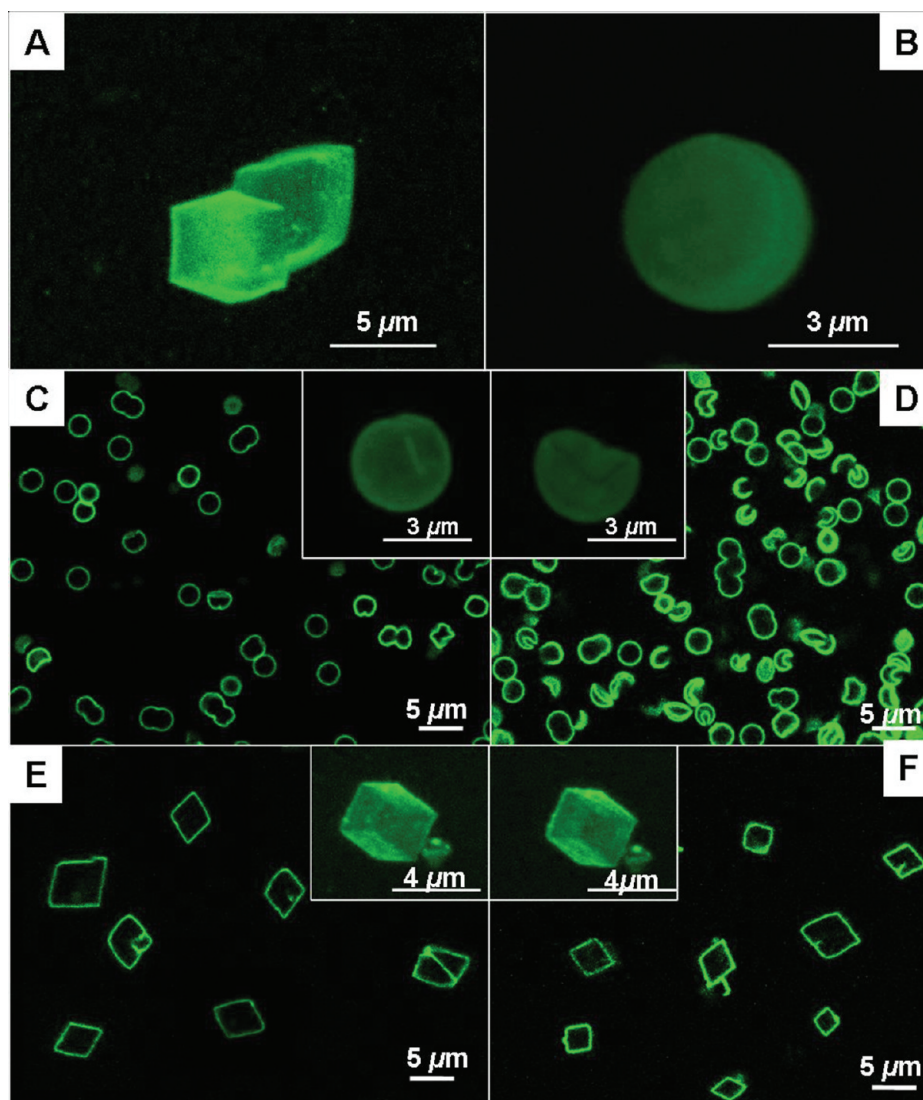


Figure 2. Confocal images of three dimensional (3D) reconstructed cubic (CdCO_3 cores) (A) and spherical (SiO_2 cores) (B) microcapsules in buffer pH 6. Deformations of $\text{PEI}(\text{TA}/\text{PVPO})_4$ microcapsules in the presence of dextran-70 kDa. Spherical microcapsules at 2% (C) and 6% (D) of dextran and cubic microcapsules at 2% (E) and 6% (F) dextran concentration. Insets demonstrate 3D images of deformed microcapsules.

three times with phosphate buffer. To etch out silica cores, the microparticles with the deposited multilayers were exposed to 8% hydrofluoric acid solution (HF) overnight followed by dialysis in Nanopure water for 36 h with repeated change of water. The CdCO_3 cores were dissolved by shaking the coated particles dispersion for four hours in 0.8 M HCl solution yielding LbL shaped hollow capsules. The dispersions of the capsules were then dialyzed against water for 3 days.

Measurements. Topographical and phase images of the surface morphology of swollen and dried capsules were obtained under ambient conditions in the tapping and phase modes in fluid and in air, respectively, using a Dimension 3000 atomic force microscope (AFM) according to established procedures.^{49–53} Samples were prepared by placing a droplet of capsule suspension onto a precleaned silicon wafer and drying in air prior to AFM imaging. For imaging in liquid, a drop of buffer solution was placed on the predried capsules. To prevent water evaporation, the buffer solution was added to the sample carefully during scanning. The capsule wall thickness was determined as half of the height of the collapsed flat regions of dried and swollen capsules from bearing analysis from NanoScope software to generate height histograms.

The force–volume (FV) mode, which utilizes the collection of the force–distance curves over selected surface areas, was used for calculation histograms of elastic modulus and reduced adhesive forces.

For micromapping, we used a $1 \mu\text{m} \times 1 \mu\text{m}$ selected surface area. Data collected was processed using micromechanical analysis (MMA) software.^{54,55} A special cantilever holder has been utilized for in-liquid measurements. AFM tip shape was determined by scanning a reference sample with gold nanoparticles. The value of microcantilever spring constant (0.046 N/m) has been obtained from thermal tuning.

Confocal images of capsules were obtained with a LSM 510 NLO META UV–Vis inverted confocal laser scanning microscope equipped with 63×1.4 oil immersion objective lens (Zeiss). The excitation/emission wavelengths were 488 and 515 nm. A drop of a dispersion of hollow capsules was added to several Lab-Tek chambers (Electron Microscopy Sciences), which were then filled with aqueous solution. Capsules were allowed to settle and then were analyzed. The solution of FITC labeled capsules was mixed with an equal amount of dextran-70 000 solution of different concentrations for osmotic pressure deformational tests. The total number of capsules counted for each dextran-70 000 concentration was at least 100.

Experiments on permeability were performed using confocal laser scanning microscopy (CLSM) with photobleaching of FITC fluorescent molecules inside the capsule with fluorescent recovery after photobleaching (FRAP).⁵⁶ Hollow capsules solution (100 mL) was combined with 200 mL of 1 mg mL^{-1} FITC-labeled dextran solution (pH = 6) and allowed to settle in a Lab-Tek chamber glass

cell for 3 h. A laser beam (488 nm) was focused within a region of interest inside a capsule and pulsed at 100% intensity to photobleach the dye molecules. Each experiment started with 3 prebleached image scans followed by 25–35 bleach pulse exposures of 3 ms each. The bleaching time was adjusted to ensure complete photobleaching of FITC-dextran inside the capsule. The fluorescence recovery was monitored by capturing 30 scans of 3 ms exposure at low laser intensity. The recovery was considered complete when the intensity of the photobleached region stabilized. Analysis of the recovery curves was conducted using a usual procedure.⁵⁷

RESULTS AND DISCUSSION

Spherical and Cubic Microcapsules under Osmotic Pressure. Original microcapsules of spherical and cubic shapes have been discussed in detail in earlier studies⁴⁴ (examples of confocal images in Figure 2). To test their mechanical stability, we placed capsules in a solution of 70 kDa dextran to create osmotically driven deformations (Figure 2). As has been observed, spherical microcapsules produced on silica cores (later referred as spherical capsules) start buckling at 2% and completely collapse at 6% dextran concentration. In contrast to spherical microcapsules, cubic microcapsules fabricated on CdCO₃ templates (referred below as cubic capsules) do not demonstrate any buckling or collapse at high concentrations of dextran. This confirms that spherical and cubic microcapsules have significantly different properties, in spite of the fact that both microcapsules are assembled from identical components.

Shell permeability was monitored using FITC-dextran of various molecular weights as a fluorescent probe. Capsules were considered impermeable for the probe if the ratio of intensities from capsule interior to bulk solution was less than 0.5 during 15 min after the fluorescent probe solution was mixed with capsules as has been suggested in the literature.⁵⁸ Table 1

Table 1. Permeability of PEI-(TA/PVPON)₄ Capsules Fabricated on Various Cores to FITC-Labeled Dextran with Different Molecular Weights^a

capsule	<i>M_w</i> (kDa)								
	4	10	20	40	70	150	250	500	2000
spherical-SiO ₂	+	+	+	–	–	–	–	–	–
cubic-CdCO ₃	+	+	+	+	+	+	+	+	+
spherical-MnCO ₃	+	+	+	+	+	+	+	–	–
cubic-MnCO ₃	+	+	+	+	+	+	+	–	–

^a "+" permeable; "–" impermeable.

compares the permeability of the dextrans through the shells made on various templates. Shells fabricated on SiO₂ cores have molecular weight cut off around 40 kDa. However, shells produced on CdCO₃ templates have much higher permeability without detectable cut off limit as a result of the permeation of labeled dextrans with the highest molecular weight exploited here (2 M).

To quantify shell permeability, we employed FRAP with fluorescent-labeled dextrans (Figure 3). At low light intensity, we observed similar emission intensity from inside and outside the capsule. With increasing excitation intensity, the dye is bleached inside of capsules and the intensity restoration was analyzed to obtain diffusion coefficients (Figure 3). The diffusion coefficients obtained from recovery data were found in the wide range from 2.6×10^{-11} to 2.5×10^{-10} cm² s⁻¹ for capsules with different shapes and number of layers in shells

(Figure 4). These values are in the same order of magnitude as values previously obtained for FITC diffusion in similar shells.²⁹

As expected, the diffusion coefficient gradually decreases with the increasing number of layers suggesting the diffusion limiting permeation (Figure 4).⁵⁹ The permeability through these hydrogen-bonded shells studied here is substantially higher than the permeability through the conventional PAH/PSS shell with diffusion coefficient of a low molecular weight dye as low as $D = 8 \times 10^{-12}$ cm² s⁻¹ for comparable number of bilayers.⁶ As we previously suggested,⁴⁸ the high permeability of these ultrathin shells is attributed to the loose, porous morphology of the TA/PVPON LbL shells, which are characteristic of weak hydrogen-bonded systems.⁶⁰

Next, it is remarkable that cubic capsules have higher permeability than spherical capsules and are fully permeable for dextrans with much larger sizes. In fact, we used 4, 70, 250, and 500 kDa fluorescently labeled dextrans to examine diffusive properties of the cubic capsules (Figure 4). The diffusion coefficient reaches 2.5×10^{-10} cm² s⁻¹ for 4 kDa dextran and 4 bilayer shells, which is five times higher than that for shells of spherical capsules. As expected, the lowest diffusion coefficient was found for 500 kDa dextran and shells composed of 6 bilayers (Figure 4).

As molecular weight of dextran increases, the diffusion coefficient noticeably decreases (Figure 4). These results are in agreement with the previously reported results for spherical capsules.^{6,29} Number of bilayers has a slight effect on diffusion rate of dextran molecules with decreasing diffusion for thicker shells, but in most cases, the diffusion coefficient values fall within the same range as defined by the standard deviation (Figure 4). Considering the fact that dextran molecules with the highest molecular weight were able to permeate the shells of cubic microcapsules, it is impossible to estimate pore size of the shells because of its large dimensions, which exceed 35 nm, which is the hydrodynamic diameter of 500 kDa dextran. This pore size for shells of cubic capsules is more than an order of magnitude larger than that for spherical microcapsule shells with pore size of around 2 nm.

The observed significant differences in shell permeability as reflected by diffusion coefficients and pore sizes for LbL shells of spherical and cubic capsules can be related to differences in shell morphologies caused by different core release mechanisms for the cubic and spherical cores, as will be discussed next.

Morphology of LbL Shells of Spherical and Cubic Capsules. The overall buckled shape and fine morphology of collapsed spherical and cubic LbL microcapsules have been observed with AFM imaging at different scales in the dried state (Figure 5 and Figure 1S in the Supporting Information). Large scale images show common collapsed morphologies, which resemble the original shapes with random wrinkling as reported in literature for LbL capsules.⁴⁸

High resolution AFM images show common fine grain morphology with dimensions well below 50 and 100 nm for cubic and spherical shells, respectively (Figure 5 and Figure 1S, Supporting Information). Thus, surface topography of a swollen LbL shells shows excessive microroughness within 6–14 nm, as measured within 300 nm × 300 nm surface areas (Table 2). Such morphology is a common trend for hydrogen bonded LbL films, as reported in literature, but the microroughness values are several times higher than those normally measured for hydrogen bonded planar LbL films, as assembled (usually within 2–5 nm), which reflect additional distortions

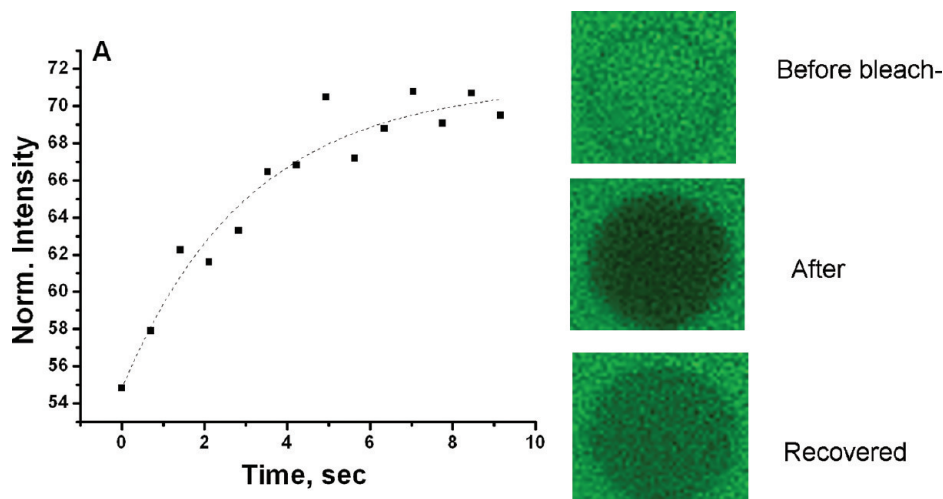


Figure 3. FRAP for spherical PEI(TA/PVPON)₄ microcapsules produced on SiO₂ cores with FITC-dextran-4 kDa.

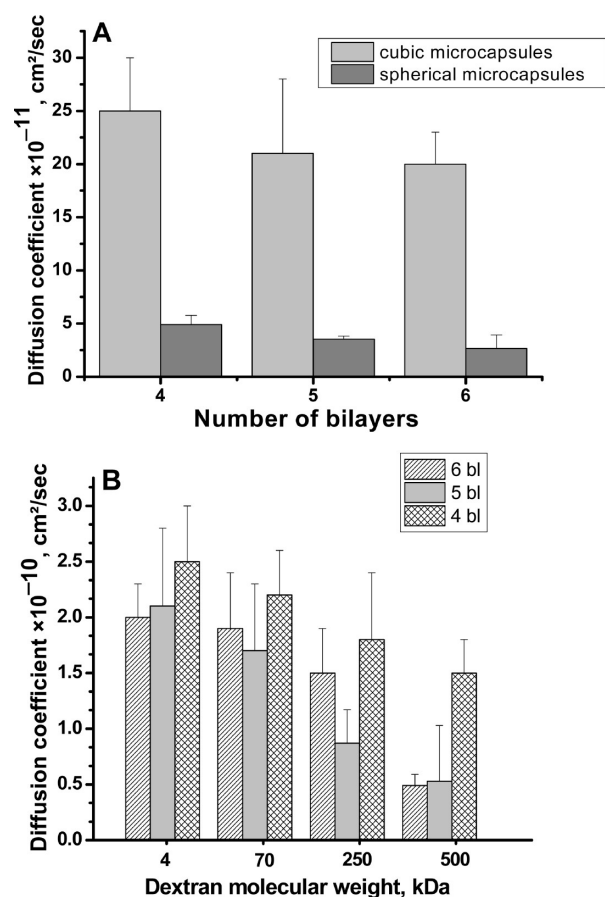


Figure 4. Diffusion coefficient of 4 kDa dextran for the spherical and cubic microcapsules versus the number of the bilayers (A); diffusion coefficient of the cubic microcapsules for dextrans of different molecular weights (B).

introduced by core dissolution and release of residuals through LbL shells.

Finally, the shell thickness in the dry state is within 13–15 nm for four-bilayer LbL shells and increases dramatically (3-fold) after swelling in the wet state (Table 2). The overall thickness of wet LbL shells with four bilayers is around 35 nm for spherical microcapsules and increases to 41 nm for LbL shells of cubic capsules (Table 2). Such a shell thickness

corresponds to a single bilayer thickness of around 10 nm, which is a common value for PVPON-based LbL films in the swollen state.⁶¹

Mechanical Properties of Spherical and Cubic LbL Shells. Next, we examined mechanical properties of LbL shells of spherical and cubic microcapsules in dry and wet states by using surface force spectroscopy (SFS) technique, according to a standard protocol.^{50,55,62} The microcapsules were casted under identical conditions on silicon substrates. The SFS method is able to probe the local elastic properties and adhesive forces of polymer films with nanoscale lateral and vertical resolution^{55,63} and has been applied to LbL shells as well as films.^{61,64}

In the dry state, the value of the elastic modulus for LbL shells was measured to be around 600 MPa, which is well below that measured for regular polyelectrolyte LbL films (within 1 to 5 GPa).⁶⁵ Reduced stiffness values measured here are caused by weak bonding and residual water content and are close to that measured earlier for similar planar hydrogen-bonded LbL films, indicating that core release process does not affect the elastic properties of LbL assemblies in the dry, collapsed state.⁶¹

A 3-fold increase in the shell thickness caused by swelling of LbL shells in water results in a significant, more than 2 orders of magnitude, reduction of the elastic modulus to the values in the low MPa range (Table 2). These values are common for highly compliant swollen gel materials and swollen LbL films with high content of water (estimated to be around 96% for LbL shells in this study).⁶¹ Indeed, the softening of multilayer shells caused by solvent post-treatment correlates with significant changes in the morphology of the shells and the formation of larger pores.⁶⁶ The significant softening of swollen PAH/PSS shells was explained by large pore formation and by the reduction of component interactions and packing density.

The histograms of the surface distribution of the elastic modulus and the adhesive forces for LbL shells from cubic microcapsules as determined via SFS technique over several selected surface areas of 1 $\mu\text{m} \times 1 \mu\text{m}$ in liquid environments are presented in Figure 6. This elastic modulus histogram shows fair uniformity of the elastic properties with deviation below 10% with the average elastic modulus of 0.61 ± 0.08 MPa. Some higher range contributions come from wrinkled shell areas. The surface distribution of adhesive forces is fairly

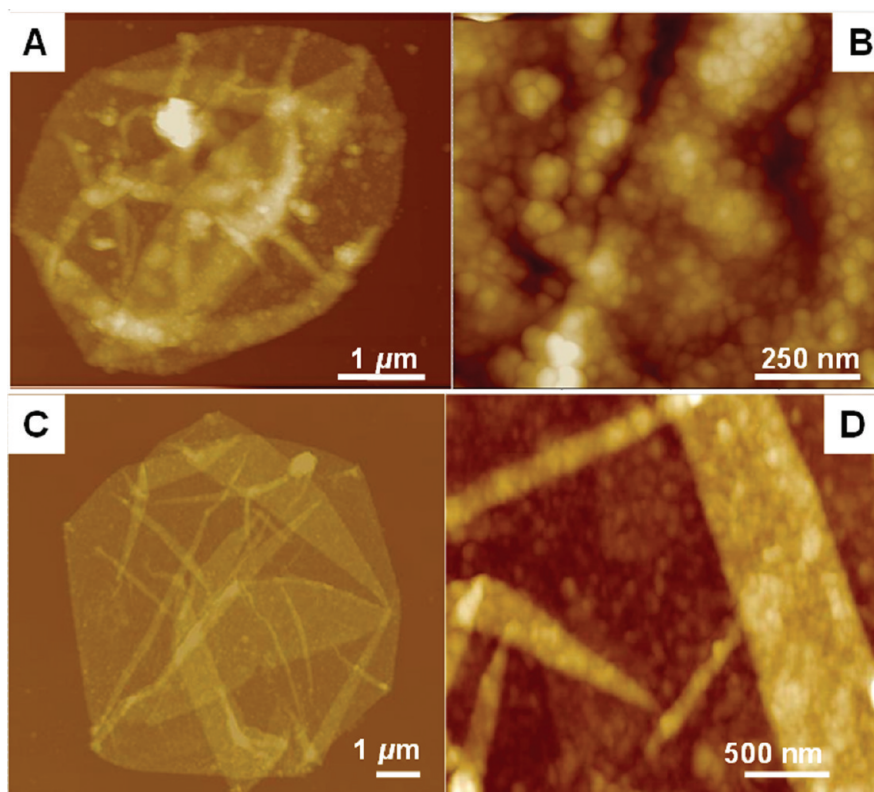


Figure 5. AFM topography images of 4-bilayer spherical (A, B) and cubic (C, D) microcapsules in dry state. Z-scales are 500 nm (A), 100 nm (B), 300 nm (C), and 120 nm (D).

Table 2. Thickness, Microroughness, and Young's Modulus of Cubic (CdCO_3 Cores) and Spherical (SiO_2 Cores) LbL Shells (All Shells Contain Four Bilayers) in Dry and Wet States

state	capsule type	thickness (nm)	microroughness (nm)	elastic modulus (MPa)
dry	spherical PEI(TA/PVPON-1300 kDa) ₄	15.0 ± 1.5	4.0 ± 0.8	600 ± 200
	cubic PEI(TA/PVPON-1300 kDa) ₄	12.7 ± 1.5	4.2 ± 0.6	600 ± 200
wet	spherical PEI(TA/PVPON-1300 kDa) ₄	35.0 ± 3.5	14.8 ± 2.3	4.3 ± 0.4
	cubic PEI(TA/PVPON-1300 kDa) ₄	41.0 ± 2.5	6.0 ± 1.4	0.8 ± 0.2

wide due to highly variable contributions from uneven buckled, depleted, and flat surface areas of collapsed shells.

The representative examples of the force–distance curves employed for elastic modulus calculations obtained by averaging over multiple probing points are presented in Figure 7. As seen, the slopes of the force–distance curves after physical contact differ significantly between cubic and spherical microcapsule shells in contrast to similar and very low adhesion. The similar pull-off forces for LbL shells of cubic and spherical microcapsules reflect identical chemical composition of the topmost layer and similar topographical landscape.

The deformational behavior of LbL shells can be quantified by converting force–distance data to loading curves, which are represented in Hertzian coordinates in Figure 2S in the

Supporting Information. The loading curves derived for both cubic and spherical microcapsules in Hertzian coordinates show the linear behavior with very different slopes for a majority of the deformational range that indicates the purely elastic deformation (Figure 2S, Supporting Information).^{67,68} In addition, as can be seen from the loading curves, the penetration depth under these loading conditions is confined to ~10% (~3 nm) of the total shell thickness, which precludes any influence of the stiff silicon substrate on measured values.⁵⁵

The elastic modulus for the LbL shells for cubic and spherical microcapsules estimated from the slopes using the Sneddon's model were 0.61 ± 0.08 MPa and 4.3 ± 0.4 MPa, respectively (Table 2). Similar values of the elastic modulus around 1 MPa were reported by Boudou et al.⁶⁹ for PE multilayer films with natural components such as poly(L-lysine)/hyaluronan, chitosan/hyaluronan, and PAH/poly(L-glutamic acid), as measured by AFM nanoindentation method. However, a higher elastic modulus of 600 MPa was obtained by Elsner et al. for swollen hydrogen-bonded PMAA/PVPON multilayer in buffer.¹⁴ The range of values of 100–200 MPa for various LbL shells was reported by Vinogradova et al.,⁷⁰ who determined elastic properties using both AFM deformation and osmotic swelling. The much higher values of 1.5–2 GPa were measured by Dubreuil and co-workers for PAH/PSS microcapsules by osmotic-driven collapse.⁷¹

In addition, to verify that core material was completely removed and the capsule properties were not affected by remaining cations, we conducted energy-dispersive X-ray spectroscopy (EDX) analysis of dried capsules (Figure 4S, Supporting Information). Within accessible sensitivity (<0.5%) EDX showed no distinct signs of Cd^{2+} present in the shell thus

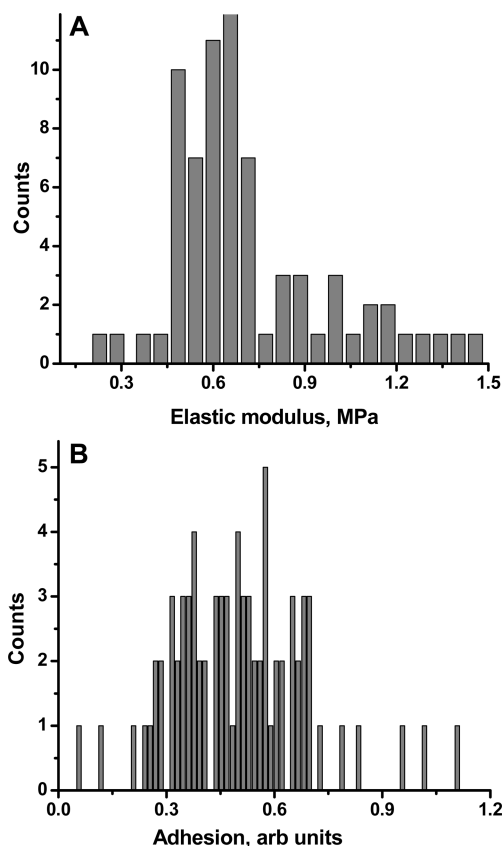


Figure 6. Histograms of the surface distribution of the elastic module (A) and adhesive force (B) of swollen four-bilayer LbL shell of cubic microcapsule. Histograms are collected at $1 \mu\text{m} \times 1 \mu\text{m}$ surface area.

leaving the question of role of the residual ion presence within the LbL shells open.

■ GENERAL DISCUSSION AND CONCLUSIONS

In our study, we focused on LbL shells produced from the same polymer systems (TA/PVPON) using two types of inorganic templates (spherical silica particles and cubic CdCO_3 particles). We aimed on demonstrating how the nature of the core and its release mechanism change the properties of the resultant LbL shells. We concluded that capsules produced on SiO_2 and CdCO_3 cores with different mechanisms of core dissolution resulting in the formation of *two uniquely different LbL shells* with dramatically altered mechanical properties and permeability as is summarized below.

Comparative analysis of all major characteristics of LbL shells of spherical and cubic microcapsules summarized and highlighted in Figure 8 shows dramatic and consistent differences in physical properties which can be related to differences in shell morphology. As shown, LbL shells of cubic microcapsules are slightly thicker than shells of regular spherical microcapsules due to the formation of larger pores during core dissolution process with large CO_2 production. In turn, this higher porosity causes a dramatic increase in the permeability and accompany significant softening of the shells.

Indeed, as has been observed in a recent study, the elastic modulus linearly depends upon porosity with a large decrease from 9 to 0.6 GPa as the porosity increases from 0% to 50%.⁷² Such results have been confirmed by Phani and Niyogi semianalytical model and by finite-element computation for the thin polymer films at low porosity.⁷³ According to Hariri

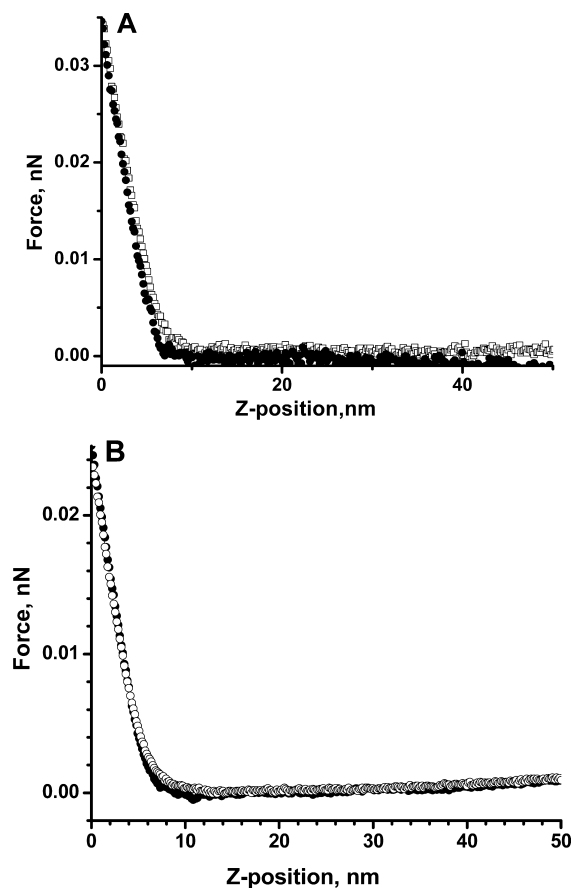


Figure 7. Force–distance curves for the swollen four-bilayer LbL shells for cubic (A) and spherical (B) microcapsules. Closed and open circles correspond to the approaching and retracting cycles, respectively.

and Schlenoff the porosity determines the amount of water in the swollen polyelectrolyte complexes that consequently control the level of the film softening.⁷⁴

Stretching of the shells due to the formation of the sharp edges on inorganic cores could also have an effect on the pore distribution and its shape leading to the increased transport through the shell.⁶⁶ As was shown by Greene et al. the pore stretching directed the flow of the interstitial fluid into the contact region thereby significantly improving the mass transport through the membrane.⁷⁵ Matsuyama et al. showed that the stretched membrane with anisotropic pore possess higher rejection coefficients for nanoparticles.^{76,77} Mertz et al. examined critical stretching at which the LbL multilayers release the fluorescein caused by the formation of anisotropic pores.⁷⁸

To exclusively study the effect of template shape, spherical and cubic microcapsules have also been fabricated using similar core materials. CaCO_3 particles of various shapes could be used for this purpose, but this type of templates has rough surface with inner cavities, connected with the outer surface through the pores.⁷⁹ Such surface morphology will affect microcapsule shell properties, resulting in fabrication of porous shells with different morphology.

Therefore, for comparative purposes, we exploited different MnCO_3 cores that can be made to have spherical and cubic shapes with identical chemical composition and dissolution process, which will affect the capsule shell properties in a

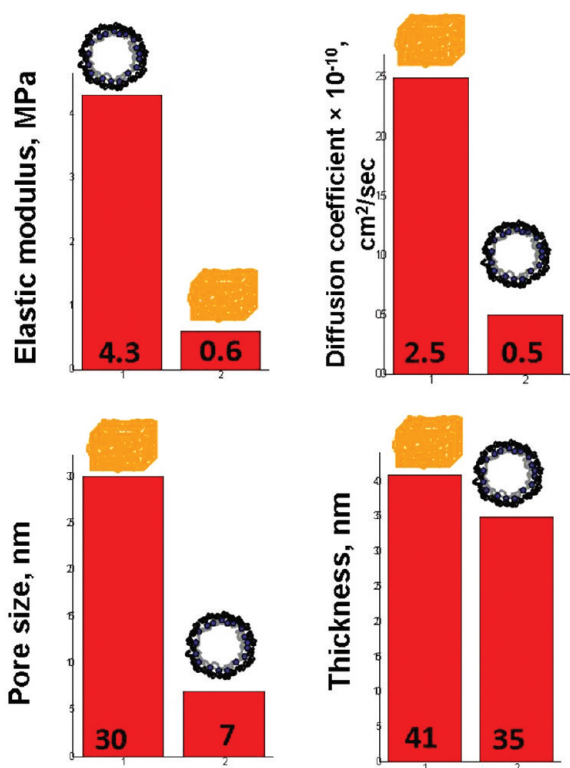


Figure 8. Elastic moduli, diffusion coefficients, thicknesses and pore size of the 4-bilayer LbL shells for cubic and spherical microcapsules in wet state. Schematic illustrations correspond to the shells of the spherical and cubic microcapsules (numbers are shown for clear comparison).

similar way. We fabricated MnCO_3 cores as a mixture of cubic and spherical particles (Figure 9 and Figure S5, Supporting Information).⁴⁷ These cores were utilized to produce capsules with different shapes but identical release procedures. Since the cores have identical chemical composition, they undergo similar dissolution processes under acidic conditions. The FRAP permeability studies revealed that both spherical and cubic capsules have similar permeability with the molecular weight cut off close to 250 kDa which is intermediate to that discussed above (Table 1). This result indicates that core material and release procedure are more crucial for controlling physical properties of final microcapsules with different shapes. On the other hand, EDX analysis showed no detectable levels of residual Mn^{2+} ions in the LbL shell after core removal (Figure

6S, Supporting Information), thus leaving the role of the possible ion cross-linkings open for future studies.

In conclusion, we revealed dramatically different mechanical properties and permeability of hydrogen-bonded LbL shells of microcapsules fabricated on different cores with different release mechanisms. As we observed, the LbL shells of cubic microcapsules are considerably softer than LbL shells for spherical microcapsules. Moreover, they show much higher permeability and porosity caused by inorganic core dissolution process with excessive gas release as well as some stretching of shells assembled around sharp edges of cubic cores. Thus, the template type might dramatically alter the mechanical properties, permeability, and morphology of LbL shells. The understanding of microcapsules' elasticity and shell permeability in conjunction with the nature of sacrificial cores is extremely important for a variety of practical applications such as the design of controlled loading and unloading microcontainers for drug delivery and targeting.

■ ASSOCIATED CONTENT

📄 Supporting Information

AFM topography images of dried capsules, the loading curves, FRAP, and EDX data for cubic capsules. This information is available free of charge via the Internet at <http://pubs.acs.org/>.

■ AUTHOR INFORMATION

Corresponding Author

*E-mail: Vladimir@mse.gatech.edu.

Author Contributions

†Both of these authors contributed equally to this study.

Notes

The authors declare no competing financial interest.

■ ACKNOWLEDGMENTS

This work was supported by the U.S. Department of Energy, Office of Basic Energy Sciences, Division of Materials Sciences and Engineering under Award No. DE-FG02-09ER46604. The authors are thankful to Jeffrey Lin, Zachary Combs, and Neal Holland for technical support.

■ REFERENCES

- (1) Caruso, F.; Caruso, R. A.; Möhwald, H. *Science* **1998**, *282*, 1111–1114.
- (2) Donath, E.; Sukhorukov, G. B.; Caruso, F.; Davis, S. E.; Möhwald, H. *Angew. Chem., Int. Ed.* **1998**, *37*, 2201–2205.

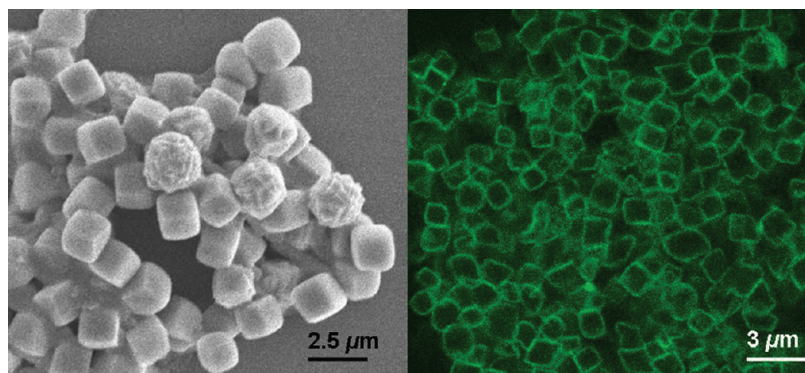


Figure 9. SEM image of mixed spherical and cubic MnCO_3 cores (left) and corresponding confocal image of microcapsules (right).

- (3) Volodkin, D.; Skirtach, A.; Mohwald, H. *Adv. Polym. Sci.* **2010**, *239*, 1–27.
- (4) Sukhorukov, G.; Möhwald, H. *Trends Biotechnol.* **2007**, *25*, 93–98.
- (5) Voigt, A.; Buske, N.; Sukhorukov, G. B.; Antipov, A. A.; Leporatti, S.; Lichtenfeld, H.; Baumler, H.; Donath, E.; Mohwald, H. *J. Magn. Magn. Mater.* **2001**, *225*, 59–66.
- (6) Antipov, A. A.; Sukhorukov, G. B.; Donath, E.; Mohwald, H. *J. Phys. Chem. B* **2001**, *105*, 2281–2284.
- (7) Antipov, A. A.; Sukhorukov, G. B.; Fedutik, Y. A.; Hartmann, J.; Giersig, M.; Mohwald, H. *Langmuir* **2002**, *18*, 6687–6693.
- (8) Lvov, Y.; Antipov, A. A.; Mamedov, A.; Mohwald, H.; Sukhorukov, G. B. *Nano Lett.* **2001**, *1*, 125–128.
- (9) Sukhorukov, G. B.; Rogach, A. L.; Garstka, M.; Springer, S.; Parak, W. J.; Munoz-Javier, A.; Kreft, O.; Skirtach, A. G.; Susha, A. S.; Ramaye, Y.; Palankar, R.; Winterhalter, M. *Small* **2007**, *3*, 944–955.
- (10) Stadler, B.; Price, A. D.; Chandrawati, R.; Hosta-Rigau, L.; Zelikin, A. N.; Caruso, F. *Nanoscale* **2009**, *1*, 68–73.
- (11) Lou, X. W.; Archer, L. A.; Yang, Z. *Adv. Mater.* **2008**, *20*, 3987–4019.
- (12) Martinez, C. J.; Hockey, B.; Montgomery, C. B.; Semancik, S. *Langmuir* **2005**, *21*, 7937–7944.
- (13) Lou, X. W.; Wang, Y.; Yuan, C.; Lee, J. Y.; Archer, L. A. *Adv. Mater.* **2006**, *18*, 2325–2329.
- (14) Elsner, N.; Kozlovskaya, V.; Sukhishvili, S. A.; Fery, A. *Soft Matter* **2006**, *2*, 966–972.
- (15) Ma, H.; Cheng, F. Y.; Chen, J.; Zhao, J. Z.; Li, C. S.; Tao, Z. L.; Liang, J. *Adv. Mater.* **2007**, *19*, 4067–4070.
- (16) Delcea, M.; Yashchenok, A.; Videnova, K.; Kreft, O.; Möhwald, H.; Skirtach, A. G. *Macromol. Biosci.* **2010**, *10*, 465–474.
- (17) Moya, S.; Donath, E.; Sukhorukov, G. B.; Auch, M.; Baumler, H.; Lichtenfeld, H.; Möhwald, H. *Macromolecules* **2000**, *33*, 4538–4544.
- (18) Khopade, A. J.; Caruso, F. *Biomacromolecules* **2002**, *3*, 1154–1162.
- (19) Shchukin, D. G.; Shutava, T.; Shchukins, E.; Sukhorukov, G. B.; Lvov, Y. M. *Chem. Mater.* **2004**, *16*, 3446–3451.
- (20) Schuler, C.; Caruso, F. *Biomacromolecules* **2001**, *2*, 921–926.
- (21) Fischlechner, M.; Zschoring, O.; Hofmann, J.; Donath, E. *Angew. Chem., Int. Ed.* **2005**, *44*, 2892–2895.
- (22) Ariga, K.; Ji, Q.; Hill, J. P. *Adv. Polym. Sci.* **2010**, *229*, 51–87.
- (23) Jiang, C.; Tsukruk, V. V. *Adv. Mater.* **2006**, *18*, 829–840.
- (24) Decher, G.; Schlenoff, J. B. In *Multilayer Thin Films—Sequential Assembly of Nanocomposite Materials*; Wiley-VCH: Weinheim, Germany, 2003.
- (25) Kharlampieva, E.; Sukhishvili, S. A. *J. Macromol. Sci., Polym. Rev.* **2006**, *46*, 377–395.
- (26) Fernandes, P. A. L.; Delcea, M.; Skirtach, A. G.; Möhwald, H.; Fery, A. *Soft Matter* **2010**, *6*, 1879–1883.
- (27) Kim, B. S.; Lebedeva, O. V.; Park, M. K.; Knoll, W.; Caminade, A. M.; Majoral, J. P.; Vinogradova, O. I. *Polymer* **2010**, *51*, 4525–4529.
- (28) Choi, R.; Suntivich; Plamper, F. A.; Synatschke, C. V.; Müller, A. H. E.; Tsukruk, V. V. *J. Am. Chem. Soc.* **2011**, *133*, 9592–9606.
- (29) Carter, J. L.; Drachuk, I.; Harbaugh, S.; Kelley-Loughnane, N.; Stone, M.; Tsukruk, V. V. *Macromol. Biosci.* **2011**, *11*, 1244–1253.
- (30) Wilson, J. T.; Cui, W.; Kozlovskaya, V.; Kharlampieva, E.; Pan, D.; Qu, Z.; Krishnamurthy, V. R.; Mets, J.; Kumar, V.; Wen, J.; Song, Y.; Tsukruk, V. V.; Chaikof, E. L. *J. Am. Chem. Soc.* **2011**, *133*, 7054–7064.
- (31) Ye, C.; Shchepelina, O.; Calabrese, R.; Drachuk, I.; Kaplan, D. L.; Tsukruk, V. V. *Biomacromolecules* **2011**, *12*, 4319–4325.
- (32) Shchepelina, O.; Drachuk, I.; Gupta, M. K.; Lin, J.; Tsukruk, V. V. *Adv. Mater.* **2011**, *23*, 4655–4660.
- (33) Shchepelina, O.; Kozlovskaya, V.; Singamaneni, S.; Kharlampieva, E.; Tsukruk, V. V. *J. Mater. Chem.* **2010**, *20*, 6587–6603.
- (34) Sukhorukov, G. B.; Donath, E.; Davis, S.; Lichtenfeld, H.; Caruso, F.; Popov, V. I.; Mohwald, H. *Polym. Adv. Technol.* **1998**, *9*, 759–767.
- (35) Lulevich, V. V.; Andrienko, D.; Vinogradova, O. I. *J. Chem. Phys.* **2004**, *120*, 3822–3826.
- (36) Gao, C. Y.; Moya, S.; Lichtenfeld, H.; Casoli, A.; Fiedler, H.; Donath, E.; Möhwald, H. *Macromol. Mater. Eng.* **2001**, *286*, 355–361.
- (37) Gao, C. Y.; Leporatti, S.; Moya, S.; Donath, E.; Mohwald, H. *Langmuir* **2001**, *17*, 3491–3495.
- (38) Antipov, A. A.; Shchukin, D.; Fedutik, Y.; Petrov, A. I.; Sukhorukov, G. B.; Mohwald, H. *Colloids Surf., A* **2003**, *224*, 175–183.
- (39) Antipov, A. A.; Sukhorukov, G. B.; Leporatti, S.; Radtchenko, I. L.; Donath, E.; Mohwald, H. *Colloids Surf., A* **2002**, *198*, 535–541.
- (40) Ibarz, G.; Dähne, L.; Donath, E.; Möhwald, H. *Adv. Mater.* **2001**, *13*, 1324–1327.
- (41) Petrov, A. I.; Volodkin, D. V.; Sukhorukov, G. B. *Biotechnol. Prog.* **2005**, *21*, 918–925.
- (42) Sukhorukov, G. B.; Volodkin, D. V.; Gunther, A. M.; Petrov, A. I.; Shenoy, D. B.; Möhwald, H. *J. Mater. Chem.* **2004**, *14*, 2073–2081.
- (43) Kozlovskaya, V.; Yakovlev, S.; Libera, M.; Sukhishvili, S. A. *Macromolecules* **2005**, *38*, 4828–4836.
- (44) Shchepelina, O.; Kozlovskaya, V.; Kharlampieva, E.; Mao, W.; Alexeev, A.; Tsukruk, V. V. *Macromol. Rapid Commun.* **2010**, *23*, 2041–2046.
- (45) Kozlovskaya, V.; Kharlampieva, E.; Jones, K.; Lin, Z.; Tsukruk, V. V. *Langmuir* **2010**, *26*, 7138–7147.
- (46) Janecovic, A.; Matijevic, E. *J. Colloid Interface Sci.* **1985**, *103*, 436–447.
- (47) Zhu, H.; Stein, E. W.; Lu, Z.; Lvov, Y. M.; McShane, M. J. *Chem. Mater.* **2005**, *17*, 2323–2328.
- (48) Kozlovskaya, V.; Kharlampieva, E.; Drachuk, I.; Cheng, D. V.; Tsukruk, V. *Soft Matter* **2010**, *6*, 3596–3608.
- (49) Lemieux, M.; Usov, D.; Minko, S.; Stamm, M.; Shulha, H.; Tsukruk, V. V. *Macromolecules* **2003**, *36*, 7244–7255.
- (50) McConney, M. E.; Singamaneni, S.; Tsukruk, V. V. *Polym. Rev.* **2010**, *50*, 235–286.
- (51) Tsukruk, V. V.; Reneker, D. H. *Polymer* **1995**, *36*, 1791–1808.
- (52) Sidorenko, A.; Ahn, H.; Kim, D.; Yang, H.; Tsukruk, V. V. *Wear* **2002**, *252*, 946–955.
- (53) Tsukruk, V. V.; Huang, Z.; Chizhik, S. A.; Gorbunov, V. V. *J. Mater. Sci.* **1998**, *33*, 4905–4909.
- (54) Shulha, H.; Kovalev, A.; Myshkin, N.; Tsukruk, V. V. *Eur. Polym. J.* **2004**, *40*, 949–956.
- (55) Kovalev, A.; Shulha, H.; Lemieux, M.; Myshkin, N.; Tsukruk, V. V. *J. Mater. Res.* **2004**, *19*, 716–728.
- (56) Ibarz, G.; Dähne, L.; Donath, E.; Mohwald, H. *Chem. Mater.* **2002**, *14*, 4059–4062.
- (57) Glinel, K.; Dubois, M.; Verbavatz, J.-M.; Sukhorukov, G. B.; Zemb, T. *Langmuir* **2004**, *20*, 8546–8551.
- (58) Tong, W.; Gao, C.; Mohwald, H. *Chem. Mater.* **2005**, *17*, 4610–4616.
- (59) von Klitzing, R.; Mohwald, H. *Macromolecules* **1996**, *21*, 6901–6906.
- (60) Kharlampieva, E.; Sukhishvili, S. A. *Polym. Rev.* **2006**, *46*, 377–395.
- (61) Lisunova, M. O.; Drachuk, I.; Shchepelina, O. A.; Anderson, K. D.; Tsukruk, V. V. *Langmuir* **2011**, *27*, 11157–11165.
- (62) Jiang, C.; Markutsya, S.; Pikus, Y.; Tsukruk, V. V. *Nat. Mater.* **2004**, *3*, 721–728.
- (63) Tsukruk, V. V.; Sidorenko, A.; Gorbunov, V. V.; Chizhik, S. A. *Langmuir* **2001**, *17*, 6715–6719.
- (64) Müller, R.; Köhler, K.; Weinkamer, R.; Sukhorukov, G. B.; Fery, A. *Macromolecules* **2005**, *38*, 9766–9771.
- (65) Lee, D.; Cohen, R. E.; Rubner, M. F. *Langmuir* **2005**, *21*, 9651–9659.
- (66) Kim, J. W.; Fernández-Nieves, A.; Dan, N.; Utada, A. S.; Marquez, M.; Weitz, D. A. *Nano Lett.* **2007**, *7*, 2876–2880.
- (67) Chizhik, S. A.; Huang, Z.; Gorbunov, V. V.; Myshkin, N. K.; Tsukruk, V. V. *Langmuir* **1998**, *14*, 2606–2609.
- (68) Domke, R.; Radmacher, M. *Langmuir* **1998**, *14*, 3320–3325.
- (69) Boudou, T.; Crouzier, T.; Auzely-Velty, R.; Glinel, K.; Picart, C. *Langmuir* **2009**, *25*, 13809–13819.

- (70) Vinogradova, O. I.; Andrienko, D.; Lulevich, V. V.; Nordschild, S.; Sukhorukov, G. B. *Macromolecules* **2004**, *37*, 1113–1117.
- (71) Dubreuil, F.; Elsner, N.; Fery, A. *Eur. Phys. J. E* **2003**, *12*, 215–221.
- (72) Stafford, C. M.; Harrison, C.; Beers, K. L.; Karim, A.; Amis, E. J.; VanLandingham, M. R.; Kim, H. C.; Volksen, W.; Miller, R. D.; Simonyi, E. E. *Nat. Mater.* **2004**, *3*, 545–550.
- (73) Phani, K. K.; Niyogi, S. K. *J. Mater. Sci.* **1987**, *22*, 257–267.
- (74) Hariri, H. H.; Schlenoff, J. B. *Macromolecules* **2010**, *43*, 8656–8663.
- (75) Greene, C. W.; Zappone, B.; Zhao, B.; Soderman, O.; Topgaard, D.; Rata, G.; Israelachvili, J. *Biomaterials* **2008**, *29*, 4455–4462.
- (76) Matsuyama, H.; Yuasa, M.; Kitamura, Y.; Teramoto, M.; Lloyd, D. R. *J. Membr. Sci.* **2000**, *179*, 91–100.
- (77) Matsuyama, H.; Berghmans, S.; Lloyd, D. R. *Polymer* **1999**, *40*, 2289–2301.
- (78) Mertz, D.; Vogt, C.; Hemmerie, J.; Mutterer, J.; Ball, V.; Voegel, J. C.; Schaaf, P.; Lavalle, P. *Nat. Mater.* **2009**, *8*, 731–735.
- (79) Antipov, A. A.; Shchukin, D.; Fedutik, Y.; Petrov, A. I.; Sukhorukov, G. B.; Moehwald, H. *Colloids Surf., A* **2003**, *224*, 175–183.